ALEPH 2002-012
CONF 2002-002
Abstract ID = ABS296
June 28, 2002

P R E L I M I N A R Y

Measurements of α_s at Centre-of-Mass Energies between 91 and 209 GeV

The ALEPH Collaboration

Contact person Hasko Stenzel (Hasko.Stenzel@cern.ch)

Abstract

Consistent measurements of event-shape variables and α_s using the complete set of data taken with the ALEPH detector at LEP are presented. The strong coupling constant is determined from a fit of $\mathcal{O}(\alpha_s^2)$+NLLA QCD calculations to distributions of six event-shape variables at eight centre-of-mass energies. A new method is proposed to estimate theoretical systematic uncertainties. The results are compared to the expected evolution of α_s.

Contributed Paper for QCD02 and ICHEP02

1 Introduction

Studies of the structure of hadronic events collected by the ALEPH detector at LEP between 91.2 and 209 GeV centre-of-mass energy are presented. The scope of this paper is a consistent measurement of event-shape variables and determinations of α_s at LEPI and LEPII energies. In performing these determinations, the primary objective is to observe the running of the coupling with centre-of-mass energy; therefore, the analyses at each energy point are designed, as far as possible, to be coherent with each other and to have correlated systematic errors. Final results of QCD analyses will be published in an upcoming paper. The data already discussed in [1–5] up to 202 GeV have been re-processed using an improved selection as described in [6, 7]. The general theoretical framework is outlined in [8] and summarised in in Appendix A. A new study of theoretical uncertainties is included in this paper. The measurements at 130-136 GeV, at 189-192 GeV, at 196-202 GeV and at 203-209 are combined, and a re-analysis of data at the Z boson resonance is included.

This paper is organised as follows: In Section 2 a brief description of the ALEPH detector and of the overall event-selection and correction procedure is given, followed by measurements of event-shape distributions. These measurements are analysed in Section 3 to determine α_s. Systematic uncertainties of the measurements of α_s are given in Section 4. Results using different variables and different energies are combined in Section 5. A summary and conclusions are found in Section 6.

2 Experimental Procedure

A detailed description of the ALEPH detector is given in [9]. The $q\overline{q}(\gamma)$ events at LEPII are extracted by selecting hadronic events as described in Ref. [3]. Hadronic events in which a Z is accompanied by an initial state photon radiation (ISR) are then removed in a procedure that has several steps. First, ISR photons observed in the detector are identified as follows. The particles in the event are clustered into jets using the Durham algorithm [10] with a resolution parameter of $y_{\rm cut} = 0.002$. Jets are identified as dominantly electromagnetic if the fraction of the jet's energy carried by charged hadrons is less than 10% and there are either no charged hadrons or else less than half of the neutral energy is hadronic. From these 'electromagnetic jets', the photon and electron (or positron) candidates are taken as originating from an ISR photon and are removed; the latter are often the result of photon conversion in the material before the tracking chambers. Next, the invariant mass $M_{\rm vis}$ of the system of remaining particles in the event is computed; the reduced centre-of-mass energy s' is also estimated by reclustering the remaining particles into two jets and calculating s' based on the angles between them. Finally, the events with a large ISR energy component are rejected by requiring that $M_{\rm vis}/\sqrt{s} > 0.7$ or $s'/s > 0.81$. According to Monte Carlo studies based on the PYTHIA generator version 5.7 [11], the fraction of radiative events (defined by $s'/s \leq 0.81$) in the selected sample is $\sim 4\%$ at 206 GeV. It should be noted that in the calculation of the event shapes and other quantities in the final analysis, all reconstructed particles in the selected event are used.

The events passing the anti-ISR cuts still contain some background from four-fermion processes (WW, ZZ, Zγ^*). These are identified by first clustering the particles to exactly four jets with the Durham algorithm. The energies of the jets are then rescaled, keeping their directions constant, such that the total energy of the event is equal to $E_{\rm cm}$ and the total momentum is zero. The quantities

$$d^2 = \min \left[\frac{(m_{ij} - M_W)^2 + (m_{kl} - M_{\rm W})^2}{M_W^2} \right] ,$$

with M_{W}= 80.25 GeV, and

$$c_{WW} = \cos(\text{smallest interjet angle})$$

are then computed, where for d^2 the minimum value is taken among all possible choices of jet pairings ij and kl. Events are accepted as $q\overline{q}$ if $d^2 \geq 0.1$ or $c_{WW} \geq 0.9$.

The integrated luminosities and numbers of events accepted and expected are shown in Table 1. The expected number of signal events has been obtained from the program KORALZ [12], those for WW background from KORALW [13] and for the ZZ and Zγ^* backgrounds from PYTHIA. The expected background is subtracted from the distributions. The data taken at

E_{cm} (GeV)	$\int L\,dt$ (pb^{-1})	events found	events expected	expected signal	expected background
133	12.30	806	822	822	0.0
161	11.08	319	333	319	14
172	9.54	257	242	218	24
183	58.83	1319	1262	1109	153
189	174.36	3578	3578	3124	454
200	206.02	3514	3528	3005	523
206	216.19	3578	3590	3072	518

Table 1: Integrated luminosities and numbers of accepted and expected events. There is an uncertainty of 2% in the predicted numbers of events.

130 and 136 GeV are averaged into a single data set at a nominal energy of 133 GeV. Weights proportional to the luminosity are applied and distributions are corrected to 133 GeV. The same procedure has been applied to the data sets at 189 and 192 GeV (averaged into a single set at nominal $\sqrt{s}$= 189 GeV), at 196, 200 and 202 (averaged to $\sqrt{s}$= 200 GeV) and to the data taken in the range from 203 to 209 GeV (averaged to 206 GeV).

Corrections for imperfections of the detector and for the residual effects of ISR are made by means of multiplicative factors, as done in [5, 6]. These factors, which are derived from the Monte Carlo model KORALZ, are by construction approximately independent of the model used. For the simulation of hadronic final states in $\mathrm{e^+e^-}$ annihilation, JETSET version 7.4 [11] and KORALZ are essentially equivalent. KORALZ is used for the detector corrections because of its more accurate description of initial state photon radiation.

The detector systematics were, when appropriate, estimated using the Z data collected in the same year as the high-energy data. The selection cuts on track parameters were changed in the Monte Carlo until the number of events selected per unit luminosity were the same in Monte Carlo and data. These changes were then applied for Monte Carlo only to the analysis of the high-energy events, and the change in the extracted values for each event-shape variable was taken as a systematic uncertainty.

A definition of the event-shape variables studied here is given in [3]; these are thrust T [16], heavy jet mass squared M_H^2/s [17], wide and total jet broadening B_W and B_T [18], C-parameter C [19] and $-\ln y_3$ [10]. The resulting event-shape distributions are shown in Figs. 1 and 1. The Event-shape variables were measured using energy flow objects [9]: charged particle tracks and neutral energy clusters in calorimeters. To account for imperfections in the description of neutral objects, classes of objects in the range from 1 to 2 GeV were excluded from the analysis, and the change in the resulting distribution was taken as systematic error. Systematic tests of the ISR and WW rejection and the event selection cuts are performed via cut variations. The dominant

uncertainty is found to be related to the Monte Carlo description of ISR, which appears in the variation of cuts in $M_{\rm vis}$ and s'/s. All other cut variations led to small uncertainties.

The systematic uncertainty due to a residual model dependence has been estimated by comparing with the results based on correction factors derived from HERWIG version 5.9 [14] and from ARIADNE 4.10 [15].

Variations in the WW cross sections used for background subtraction by ± 2 % led to negligible uncertainties in the corrected distributions.

In the event-shape distributions, the systematic uncertainty estimates in each bin are dominated by the small changes in the selected events and tracks as cuts are varied, and hence are very much limited in statistical precision. For this reason, the estimates for neighbouring bins have been averaged in groups of three.

For the measurement of event shapes at the Z boson resonance, about 1.1 million events were selected from the running periods in 1994 and 1995. Where appropriate, the experimental systematic uncertainties were obtained in a similar way than at LEPII. The dominant experimental systematic uncertainty stems from the residual model dependence of detector corrections.

3 Measurements of α_s

Distributions of event-shape variables are used to determine the strength of strong interactions. The coupling constant α_s is determined from a fit of the perturbative QCD prediction to the measured event-shape distributions. The experimental situation at energies above $M_{\rm Z}$ is different from measurements at $M_{\rm Z}$. Statistical uncertainties are larger and background conditions are more difficult. In general theoretical uncertainties limit the precision of the measurements, except for the very small data sets at 161 and 172 GeV, where statistical errors dominate. At these energies it is particularly essential to combine measurements from different variables.

A study with Monte Carlo generated distributions revealed that the fit procedure is systematically biased towards lower values of α_s in the case of small event statistics, as encountered at 161 and 172 GeV. This bias originates from larger weights of downward fluctuating bins in the distributions compared to upward fluctuations. It can be overcome by replacing the measured statistical uncertainties of the distribution by expected statistical errors. The expected uncertainties are obtained from a large number of Monte Carlo experiments, each of the same sample size as the real data. The RMS in each bin of the Monte Carlo distributions is used in the fit procedure as statistical error. This is done for all variables at all energy points above M_Z.

Event-shape distributions are fitted in the central region of 3-jet production, where a good perturbative description is available. The fit range is placed inside a region where hadronisation corrections are well under control, where detector corrections are stable and background corrections are small. At high energies the fit range was extended into the 2-jet region in order to reduce the statistical error as much as possible. This generates larger perturbative uncertainties, which are avoided at $Q = M_{\rm Z}$ by restricting the fit range. The data are corrected for detector effects, background from 4-fermion processes and for a residual ISR contribution, as outlined in Section 2. The background from WW events is increasing with energy, and after subtraction some bins of the distribution become negative. This affects the choice of the fit range, which was restricted to regions with a good signal-to-background ratio.

Distributions of infrared- and collinear-safe observables at partonic level can be computed in perturbative QCD to second order in α_s using the ERT matrix elements [20]. In addition, the variables used in this analysis exhibit the property of exponentiation so that leading and next-to-leading logarithms can be resummed to all orders in α_s into analytic functions [21–24]. These resummed calculations, valid in the semi-inclusive 2-jet region, have to be matched to the fixed order part in order to obtain an improved prediction over the entire phase space. The renormalization scale $x_\mu = \mu/Q$ is set under nominal conditions to one. For this analysis

modified Log(R) and R [21] matching schemes are used. For convenience the formulae are given in Appendix A. A kinematic constraint is imposed such that the predicted distributions vanish at a given boundary value y_{max}. In addition, improved calculations for $-\log(y_3)$ have become available [25], which add previously missing single-logarithmic terms due to multiple gluon emission. The improved calculations have been implemented in the fit functions. It is observed that the quality of the fits to $-\log(y_3)$ improves and the fitted value of α_s is 1.5 % lower compared to the partial prediction.

All these calculations above neglect quark masses. Quark mass effects are relevant for the b-quark at M_{Z}, where the fraction of b-quarks is large in an inclusive sample, while $Q = \sqrt{s}$ is still moderate. Calculations including a quark mass indicate that the expected change in α_s is of the order of 1% at M_{Z}. The effect is scaling with m_b^2/Q^2 and decreases to 0.2-0.3 % at 200 GeV. Mass corrections were computed to second order using the matrix elements of [26]. A pole b-quark mass $\mathrm{M_b} = 5$ GeV was used and Standard Model values were taken for the fraction of b-quarks. Since no corrections are yet available for the resummed calculations, the full theoretical prediction can only account for the quark mass effect in the perturbative region. The perturbative QCD prediction is corrected for hadronisation and resonance decays by means of a transition matrix, which is computed with Monte Carlo generators. Corrected measurements of event-shape distributions are compared to the theoretical calculation at particle level.

The value of α_s is determined at each energy from a binned least-squares fit. Only statistical uncertainties are included in the χ^2 of the fit. The fit quality is good for all variables at LEPII, but inferior at LEPI for M_H and B_W. Nominal fit results are shown in Figs. 1 and 2 together with the measured distributions. The resulting measurements of $\alpha_s(Q)$ are given in Table 2 for 91.2 to 172 GeV and in Table 3 for 183 to 206 GeV. All individual measurements are also shown in Fig. 3 together with combined measurements at each energy (see below). Systematic theoretical and experimental uncertainties are discussed in the next section.

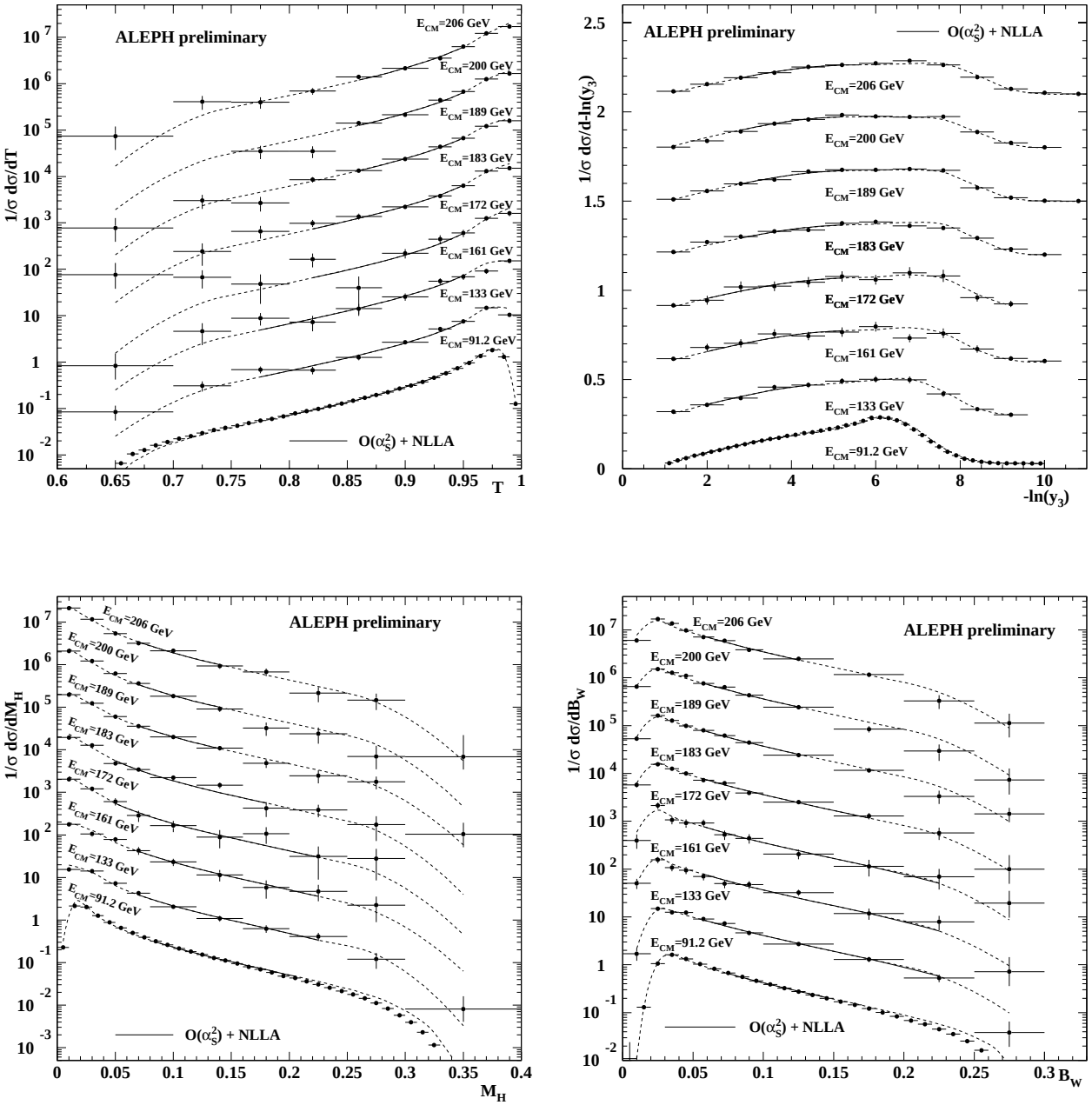

Figure 1: The measured distributions, after correction for backgrounds and detector effects, of thrust, $-\ln y_3$, heavy jet mass and wide jet broadening at energies between 91.2 and 206 GeV together with the fitted QCD predictions. The error bars correspond to statistical uncertainties. The fit ranges cover the central regions indicated by the solid line, the theoretical predictions extrapolate well outside the fitted ranges, as shown by the dotted lines. The plotted distributions are scaled by arbitrary factors.

Q = 91.2 GeV						
variable	T	$-\log y_3$	M_{H}	C	B_{W}	B_{T}
α_s	0.1264	0.1180	0.1187	0.1225	0.1163	0.1260
stat. error	0.0001	0.0002	0.0002	0.0001	0.0002	0.0001
pert. error	0.0063	0.0038	0.0043	0.0058	0.0051	0.0080
hadr. error	0.0020	0.0015	0.0037	0.0015	0.0015	0.0029
exp. syst. error	0.0008	0.0010	0.0009	0.0007	0.0006	0.0007
total error	0.0067	0.0042	0.0057	0.0061	0.0054	0.0085
Q = 133 GeV						
variable	T	$-\log y_3$	M_{H}	C	B_{W}	B_{T}
α_s	0.1208	0.1177	0.1154	0.1182	0.1157	0.1183
stat. error	0.0039	0.0046	0.0049	0.0035	0.0032	0.0029
pert. error	0.0054	0.0030	0.0036	0.0049	0.0044	0.0068
hadr. error	0.0014	0.0008	0.0025	0.0012	0.0009	0.0019
exp. syst. error	0.0011	0.0010	0.0011	0.0011	0.0005	0.0015
total error	0.0069	0.0056	0.0067	0.0063	0.0055	0.0078
Q = 161 GeV						
variable	T	$-\log y_3$	M_{H}	C	B_{W}	B_{T}
α_s	0.1222	0.1127	0.1185	0.1173	0.1103	0.1081
stat. error	0.0063	0.0072	0.0080	0.0056	0.0054	0.0046
pert. error	0.0049	0.0027	0.0034	0.0045	0.0040	0.0062
hadr. error	0.0012	0.0006	0.0021	0.0010	0.0007	0.0015
exp. syst. error	0.0011	0.0010	0.0011	0.0011	0.0005	0.0016
total error	0.0081	0.0078	0.0090	0.0074	0.0068	0.0081
Q = 172 GeV						
variable	T	$-\log y_3$	M_{H}	C	B_{W}	B_{T}
α_s	0.1113	0.1080	0.1071	0.1092	0.1060	0.1144
stat. error	0.0074	0.0083	0.0081	0.0063	0.0066	0.0067
pert. error	0.0048	0.0027	0.0034	0.0045	0.0040	0.0060
hadr. error	0.0012	0.0005	0.0019	0.0010	0.0006	0.0014
exp. syst. error	0.0011	0.0011	0.0011	0.0011	0.0006	0.0016
total error	0.0090	0.0088	0.0090	0.0078	0.0077	0.0093

Table 2: Results on $\alpha_s(Q)$ as obtained from fits to distributions of event-shape variables at 91.2, 133, 161 and 172 GeV.

Q = 183 GeV						
variable	T	$-\log y_3$	M_{H}	C	B_{W}	B_{T}
α_s	0.1130	0.1060	0.1087	0.1073	0.1054	0.1141
stat. error	0.0037	0.0037	0.0039	0.0038	0.0030	0.0031
pert. error	0.0048	0.0026	0.0032	0.0044	0.0038	0.0059
hadr. error	0.0011	0.0005	0.0018	0.0009	0.0006	0.0013
exp. syst. error	0.0012	0.0011	0.0011	0.0013	0.0005	0.0016
total error	0.0062	0.0047	0.0055	0.0060	0.0049	0.0070
Q = 189 GeV						
variable	T	$-\log y_3$	M_{H}	C	B_{W}	B_{T}
α_s	0.1164	0.1075	0.1097	0.1123	0.1066	0.1148
stat. error	0.0020	0.0023	0.0027	0.0022	0.0018	0.0020
pert. error	0.0046	0.0026	0.0032	0.0042	0.0038	0.0059
hadr. error	0.0011	0.0004	0.0017	0.0009	0.0005	0.0013
exp. syst. error	0.0011	0.0010	0.0012	0.0011	0.0005	0.0017
total error	0.0052	0.0037	0.0047	0.0050	0.0043	0.0065
Q = 200 GeV						
variable	T	$-\log y_3$	M_{H}	C	B_{W}	B_{T}
α_s	0.1114	0.1088	0.1038	0.1113	0.1039	0.1141
stat. error	0.0021	0.0022	0.0031	0.0024	0.0019	0.0021
pert. error	0.0045	0.0026	0.0031	0.0042	0.0037	0.0058
hadr. error	0.0011	0.0004	0.0016	0.0009	0.0005	0.0012
exp. syst. error	0.0011	0.0010	0.0018	0.0011	0.0005	0.0016
total error	0.0052	0.0036	0.0050	0.0050	0.0042	0.0064
Q = 206 GeV						
variable	T	$-\log y_3$	M_{H}	C	B_{W}	B_{T}
α_s	0.1088	0.1024	0.1059	0.1052	0.1028	0.1078
stat. error	0.0021	0.0023	0.0029	0.0023	0.0019	0.0021
pert. error	0.0045	0.0026	0.0031	0.0041	0.0037	0.0056
hadr. error	0.0010	0.0004	0.0016	0.0009	0.0005	0.0011
exp. syst. error	0.0011	0.0010	0.0011	0.0011	0.0005	0.0015
total error	0.0052	0.0036	0.0046	0.0049	0.0043	0.0063

Table 3: Results on $\alpha_s(Q)$ as obtained from fits to distributions of event-shape variables at 183, 189, 200 and 206 GeV.

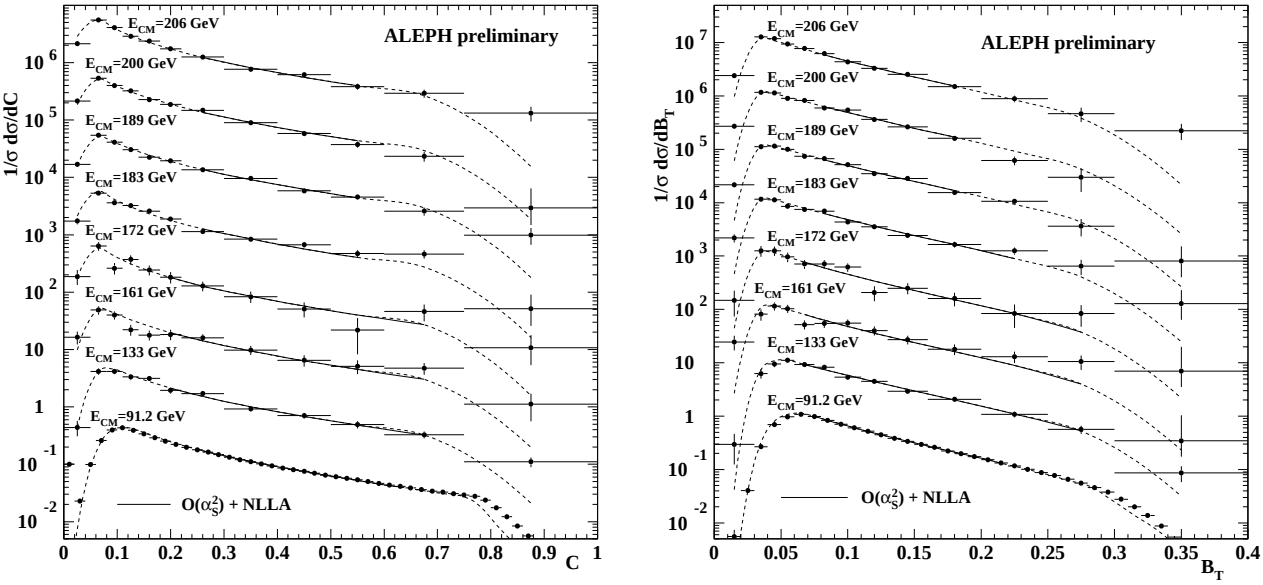

Figure 2: The measured distributions, after correction for backgrounds and detector effects, of C-parameter and total jet broadening at energies between 91.2 and 206 GeV together with the fitted QCD predictions. The error bars correspond to statistical uncertainties. The fit ranges cover the central regions indicated by the solid line, the theoretical predictions extrapolate well outside the fitted ranges, as shown by the dotted lines. The plotted distributions are scaled by arbitrary factors.

4 Systematic Uncertainties

Experimental Uncertainties

Experimental systematic uncertainties of α_s are estimated in a similar way to that for the event shapes themselves, as described in Section 2. Changes of the distributions under variations of cuts lead in general to small changes in α_s. In the fit procedure the same expected statistical error is assumed everywhere for all variants of the distribution, as outlined in Section 3. This procedure reduces purely statistical components in the real systematic effect, which are potentially large at LEPII energies. A special treatment was applied for the dominant systematic uncertainty, the variation of the combined cut in $M_{\rm vis}/\sqrt{s}$ and s'/s from 0.7/0.81 to 0.85/0.9. This cut variation entails the largest change in the number of events. The resulting error in α_s is fluctuating from one energy to another and contains obviously an irreducible statistical component. Therefore, an energy-independent luminosity-weighted average is constructed for each variable separately at energies between 133 and 206 GeV. All other components of systematic uncertainty are added in quadrature to this error. The total experimental systematic uncertainties of α_s at LEPII are between 0.5 % and 1.5 %. Those at LEPI are below 1 % and dominated by imperfections of the simulation of neutral hadronic calorimeter clusters.

Theoretical Uncertainties

A new method is applied to estimate systematic uncertainties related to the perturbative predictions. Sources of these uncertainties are the choice of the renormalization scale (x_μ) and the logarithmic rescaling factor x_L, the matching scheme and the matching modification procedure. A new test is included here for the logarithmic rescaling factor x_L. It was first proposed for jet broadening in deep-inelastic scattering [27]. The essence of this test consist in a replacement of

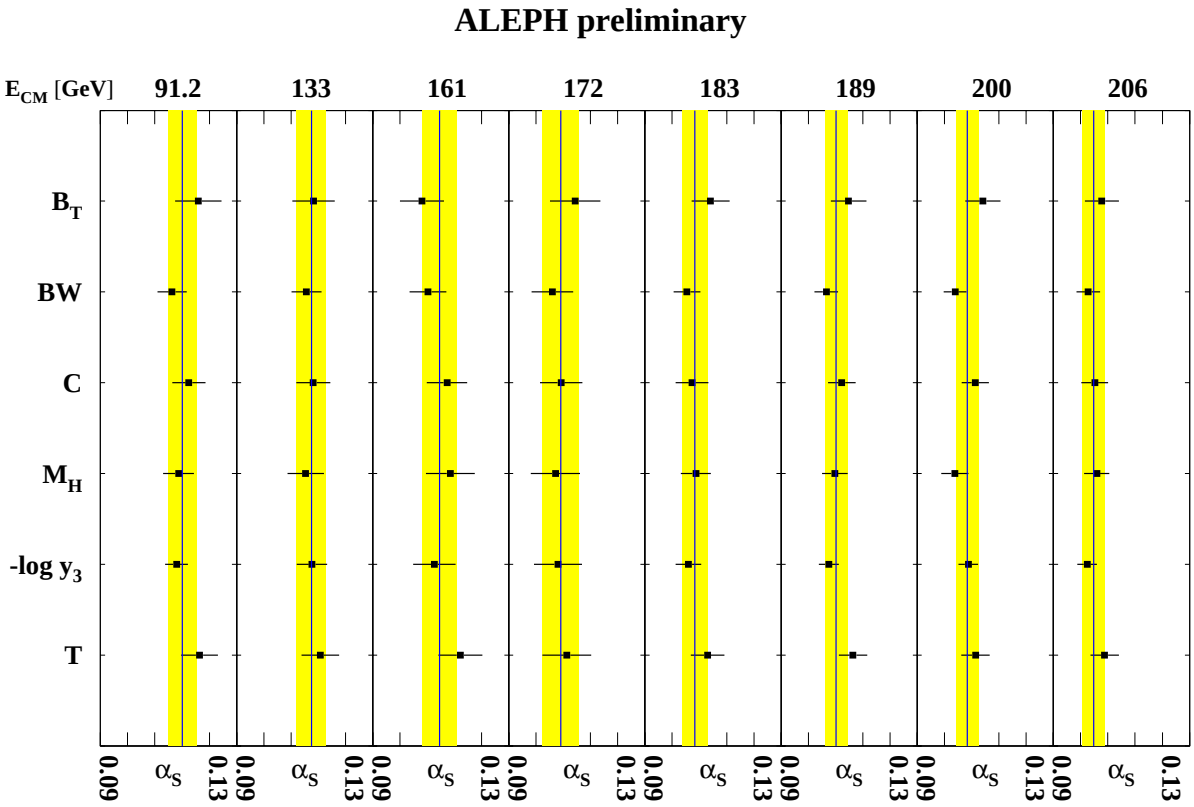

Figure 3: Summary of all individual measurements of α_s using six variables at eight centre-of-mass energies. The error bars correspond to the total uncertainties, the shaded areas to the combined measurements given in Table 4.

resummed large logarithms $L = \log(\frac{1}{y})$ (y being an event shape variable such as $1 - T$), by a rescaled variable $L \to \bar{L} = \log(\frac{1}{y \cdot x_L})$. The rescaling factor should be chosen of order unity. A variation of x_L is expected to probe missing higher orders in a different way from renormalisation scale variations. Values of x_L different from unity will entail changes of the matching formulae, which are given in Appendix A. The perturbative uncertainties are assessed as follows:

- the renormalization scale x_μ is varied between 0.5 and 2.0,
- the logarithmic rescaling factor x_L varied in between 2/3 and 3/2
  (for $-\log(y_3)$ an equivalent effect is obtained with squared endpoints, i.e. a variation from 4/9 to 9/4),
- the modified Log(R) matching scheme is replaced by the modified R matching scheme,
- the value of the kinematic constraint y_{max}, obtained with parton shower simulations, is replaced by the value of y'_{max} using matrix element calculations and
- the first degree modification of the modified Log(R) matching scheme ($p = 1$) is replaced by a second degree modification ($p = 2$).

The uncertainties in α_s corresponding to these theoretical uncertainties were previously obtained by modifying the theory (e.g. setting a different value of x_μ), and repeating the fits to the data. The quality of fits carried out with extreme variations of theoretical predictions is usually rather bad. The values for parameters determined under such conditions are less reliable.

The new method derives directly the uncertainty of α_s from the uncertainty of the theoretical prediction. It proceeds in three steps. First a reference perturbative prediction, the modified Log(R) matching scheme, is calculated for the distribution of each variable using the values of α_s measured at M_Z. Then all variants of the theory mentioned above are calculated with the same value of α_s. In each bin of the distribution, the largest upward and downward differences with respect to the reference theory are taken to define an uncertainty band around the reference theory.

In the last step, the reference theory is used again, but with a variable α_s, in order to find the range of α_s values which result into predictions inside the uncertainty band for the fit range under consideration. The largest respectively smallest allowed values of α_s fulfilling the condition finally set the perturbative systematic error. The method is illustrated in Fig. 4, taking thrust as an example.

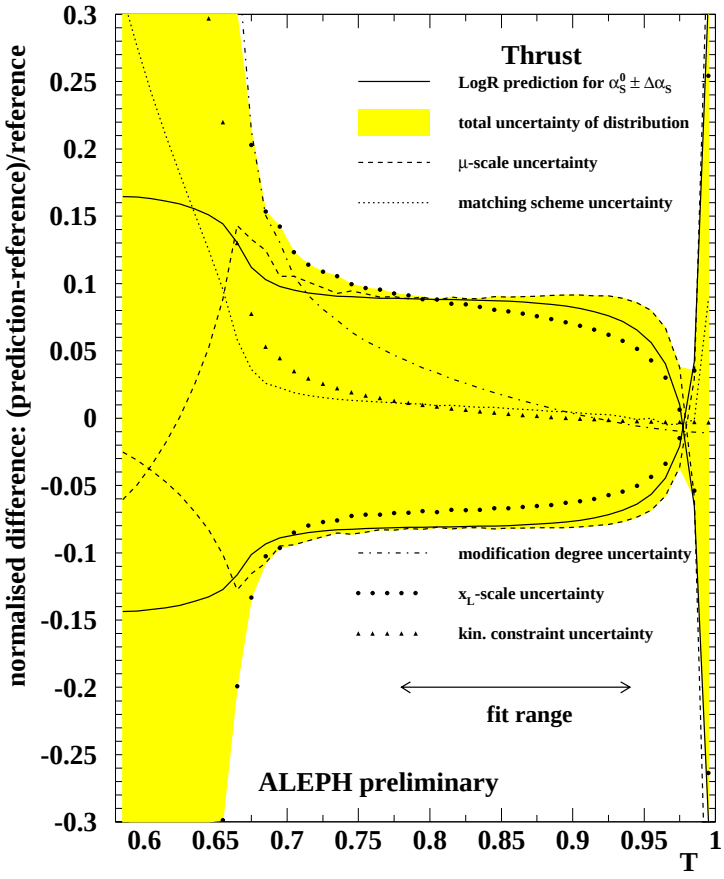

Figure 4: Theoretical uncertainties for the distribution of thrust at LEPI obtained with the measured value α_s^0. The normalised difference between various perturbative predictions with respect to a reference theory, the modified logR matching scheme, are shown. All predictions of the modified logR matching scheme with accepted values of α_s lie between the two full lines, which correspond to the total uncertainty of α_s, i.e. $\alpha_s^0 + \Delta\alpha_s$ resp. $\alpha_s^0 - \Delta\alpha_s$. The endpoints $\alpha_s^0 \pm \Delta\alpha_s$ are obtained with the condition that valid predictions must lie within the grey uncertainty band. This band comprises for a given measured value of α_s all uncertainties of the distribution. The dashed lines stem from the variation of the renormalization scale from $0.5 \leq x_\mu \leq 2.0$, the dotted line is the difference between the modified logR and modified R matching scheme, the dashed-dotted line is the difference between $p = 1$ and $p = 2$ (see text), the bullets stand for the variation of the rescaling factor x_L and the upward pointing triangles reflect the uncertainty of the choice of y_{max}.

The theoretical error depends on the absolute value of α_s, scaling approximately with α_s^3, and on the fit range. At LEPII energies the statistical fluctuations are large. In order to avoid biases from downward fluctuations, the theoretical uncertainties are calculated with the value of α_s measured at LEPI. For each variable, the corresponding measurement is evolved to the appropriate energy scale and the uncertainty is calculated for the fit range used at that energy point.

An additional error is given for the b-quark mass correction procedure. This correction is only available at $\mathcal{O}(\alpha_s^2)$, no resummed expressions are yet available. The difference in α_s obtained with and without mass corrections is taken as systematic error.

The hadronisation model uncertainty is estimated by using HERWIG and ARIADNE instead of PYTHIA for both hadronisation and detector corrections. The maximum change with respect to the nominal result using PYTHIA is taken as error. At LEPII energies the hadronisation model uncertainty is again subject to statistical fluctuations. These fluctuations are observed from one energy to the next and originate from limited statistics of correction functions. Since non-perturbative effects are expected to decrease with $1/Q$, the energy evolution of hadronisation errors has been fit to a simple $A+B/Q$ form. The fit was performed for each variable separately. In the fit procedure a weight scaling with luminosity is assigned to the hadronisation uncertainty at each energy point. This ensures that the hadronisation uncertainty at M_{Z}, which is basically free of statistical fluctuations, is not altered by the procedure.

The perturbative component of the error, which is the dominant source of uncertainty in most cases, is highly correlated between the energy points. The perturbative errors decrease with increasing Q, but faster than the coupling constant itself. The error is in general dominated by the combination of renormalisation scale and logarithmic variable rescaling uncertainties.

5 Combined Results

The measurements obtained with different variables are combined into a single measurement per energy using weighted averages. A weight is assigned to each observable dependent measurement α_s^i proportional to the inverse square of its total error $w_i \propto 1/\sigma_i^2$. The weighted average $\overline{\alpha}_s$ is then given by:

$$\overline{\alpha}_s = \sum_{i=1}^{N} w_i \alpha_s^i \quad , \tag{1}$$

and the combined statistical error is

$$\sigma_{\overline{\alpha}_s}^{stat} = \sqrt{\sum_{i\neq j}^{N} (\sigma_i w_i)^2 + 2\rho_{ij}\sigma_i w_i \sigma_j w_j} \quad . \tag{2}$$

In order to obtain the statistical error of the weighted average, the correlation coefficients ρ_{ij} are needed. This is the correlation between fits of α_s to different variables, which has been obtained by fitting a large number of Monte Carlo data samples. The linear correlation coefficient is typically 60-80 %. The correlation of systematic errors is taken into account in such a way, that the weighted average is recomputed for all variations of the analysis, and the change in α_s with respect to the nominal value is taken as error. Combined results are given in Table 4. The combined experimental systematic uncertainty at LEPII energies is obtained from a luminosity-weighted average of the uncertainties between 133 GeV and 206 GeV. They are also shown in Fig. 5, together with a fit of the QCD expectation. The curve is seen to be in excellent agreement with the measurements. It worth noting that in the definition of the χ^2 of the fit only the uncorrelated component of the errors is taken into account, which excludes the theoretical error.

Q [GeV]	91.2	133	161	172	183	189	200	206
$\alpha_s(Q)$	0.1201	0.1175	0.1145	0.1091	0.1083	0.1102	0.1083	0.1048
stat. error	0.0001	0.0027	0.0042	0.0051	0.0024	0.0015	0.0015	0.0016
pert. error	0.0050	0.0045	0.0043	0.0042	0.0039	0.0037	0.0037	0.0036
hadr. error	0.0016	0.0011	0.0009	0.0008	0.0008	0.0007	0.0007	0.0007
exp.syst. error	0.0008	0.0010	0.0010	0.0010	0.0010	0.0010	0.0010	0.0010
total error	0.0053	0.0054	0.0062	0.0067	0.0047	0.0042	0.0041	0.0041

Table 4: Combined results of $\alpha_s(Q)$ as obtained with weighted averages.

In a second step combined measurements between 133 and 206 GeV are evaluated at the scale of the Z boson mass. This is done by using the predicted energy evolution of the coupling constant at 3-loop level [28]. The evolved measurements at M_{Z} are given in Table 5. Once all measurements are evolved to the same scale, they can again be combined into a weighted average of $\alpha_s(M_{\mathrm{Z}})$, again with weights proportional to the inverse square of total errors. In contrast to the combination from different variables, the measurements here are statistically uncorrelated. Systematic error correlations are taken into account, all variations of the determination of α_s have been performed for the weighted average. The result is given in Table 6. A combination of measurements at LEPII energies without the point at M_{Z} is given as well. The total uncertainty of the combined LEPII measurement is comparable to the one including LEPI, since the perturbative uncertainties are reduced at higher energies, even after evolution to M_{Z}. The measurements at LEPI and LEPII are in good agreement with each other and with previously published ALEPH measurements of α_s [8, 29–31]. Finally as a cross-check,

Q [GeV]	91.2	133	161	172	183	189	200	206
$\alpha_s(M_{\mathrm{Z}})$	0.1201	0.1246	0.1248	0.1197	0.1199	0.1228	0.1215	0.1176
stat. error	0.0001	0.0031	0.0050	0.0061	0.0029	0.0019	0.0019	0.0020
pert. error	0.0050	0.0047	0.0047	0.0046	0.0043	0.0042	0.0041	0.0041
hadr. error	0.0016	0.0012	0.0010	0.0010	0.0009	0.0009	0.0008	0.0008
exp.syst. error	0.0008	0.0013	0.0013	0.0013	0.0013	0.0013	0.0013	0.0013
total error	0.0053	0.0059	0.0071	0.0079	0.0054	0.0048	0.0048	0.0048

Table 5: Combined results of $\alpha_s(M_{\mathrm{Z}})$ as obtained with weighted averages and evolved from $Q \to M_{\mathrm{Z}}$.

data set	LEPI + LEPII	LEPII
$\alpha_s(M_{\mathrm{Z}})$	0.1211	0.1213
stat. error	$\pm$ 0.0009	$\pm$ 0.0011
pert. error	$\pm$ 0.0044	$\pm$ 0.0043
hadr. error	$\pm$ 0.0010	$\pm$ 0.0009
exp. syst. error	$\pm$ 0.0011	$\pm$ 0.0013
total error	$\pm$ 0.0047	$\pm$ 0.0047

Table 6: Weighted average of combined measurements of $\alpha_s(M_{\mathrm{Z}})$ obtained at energies from 91.2 GeV to 206 GeV and a combined measurement without the point at M_{Z}.

another combination method was investigated. A simultaneous fit to data sets at all energies was performed. Effectively, this implies using statistical uncertainties as weights, so this result

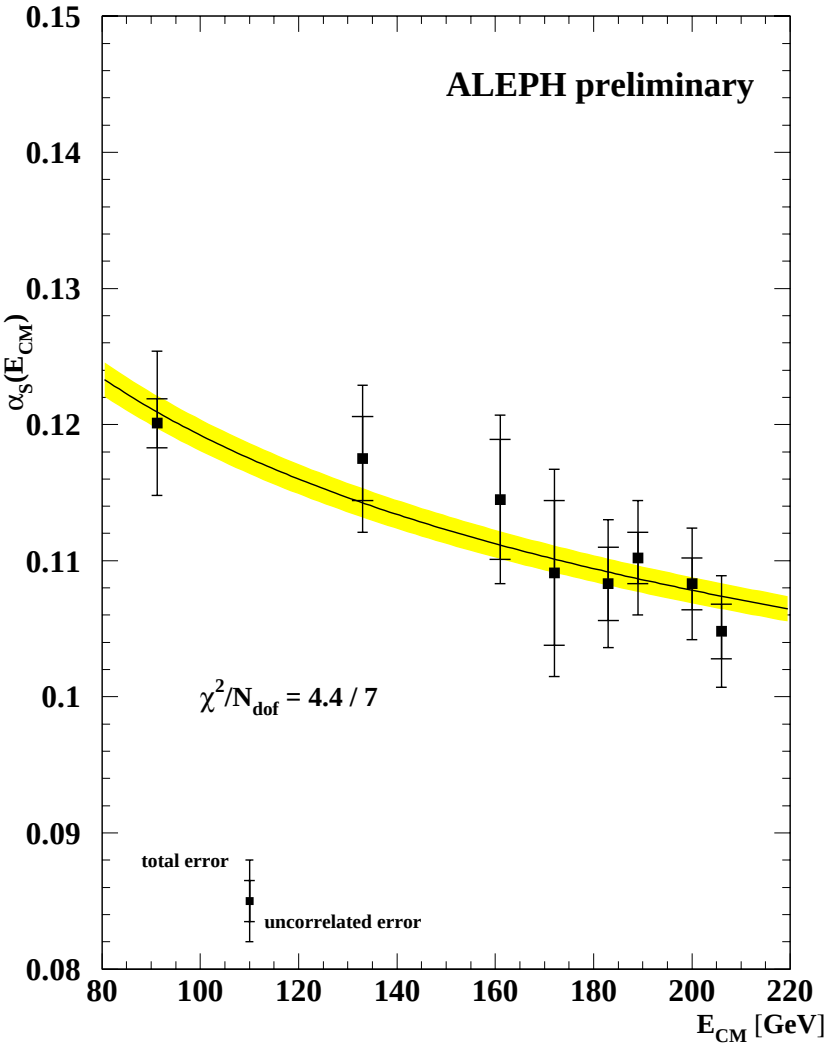

Figure 5: The strong coupling constant α_s measured between 91.2 and 206 GeV. The measurements using different event-shape variables are combined, correlations are taken into account. The outer error bars indicate the total error. The inner error bars exclude the theoretical error, which is expected to be highly correlated between the measurements. A fit of the 3-loop running formula is shown, where the hatched area corresponds to the statistical uncertainty of $\Lambda_{\overline{\rm MS}} = 245 \pm 15$ MeV.

is dominated by the precise data at $M_{\rm Z}$, and the result $\alpha_s(M_{\rm Z}) = 0.1203 \pm 0.0052$ is practically the same as without high energy data. The simultaneous fit method yields results which are again consistent with those obtained with weighted averages.

6 Conclusions

New results are presented for a consistent measurement of event-shape variables recorded by ALEPH at centre-of-mass energies between 91.2 GeV and 209 GeV. The energy evolution of the strong coupling constant α_s has been investigated.

The distributions of thrust, C-parameter, heavy jet mass, $-\ln y_3$, wide and total jet broadening have been compared to calculations of perturbative QCD, and the strong coupling constant has been measured at all energies. The new combined ALEPH result is $\alpha_s(M_{\rm Z}) = 0.1211 \pm 0.0047$. The results are found to be in good agreement with the expected energy evolution of the running coupling constant.

Acknowledgements

We wish to thank our colleagues from the accelerator divisions for the successful operation of LEP. It is also a pleasure to thank the technical personnel of the collaborating institutions for their support in constructing and maintaining the ALEPH experiment. Those of the collaboration not from member states thank CERN for its hospitality.

References

[1] ALEPH Collab., ALEPH 1998-025 CONF 1998-014 (1998).

[2] ALEPH Collab., ALEPH 1998-049 CONF 1998-023 (1998).

[3] ALEPH Collab., ALEPH 1999-023 CONF 1999-018 (1999).

[4] ALEPH Collab., ALEPH 2000-017 CONF 2000-014 (2000).

[5] ALEPH Collab., ALEPH 2000-044 CONF 2000-027 (2000).

[6] ALEPH Collab., ALEPH 2001-007 CONF 2001-004 (2001).

[7] ALEPH Collab., ALEPH 2001-062 CONF 2001-042 (2001).

[8] D. Decamp et al., ALEPH Collab., Phys. Lett. B284 (1992) 163.

[9] D. Decamp et al., ALEPH Collab., Nucl. Instr. Meth. A 294 (1990) 121;
D. Decamp et al., ALEPH Collab., Nucl. Instr. Meth. A 360 (1995) 481.

[10] S. Catani et al., Phys. Lett. B269 (1991) 432;
W.J. Stirling et al., Proceedings of the Durham Workshop, J. Phys. G: Nucl. Part. Phys. 17 (1991) 1567;
N. Brown and W.J. Stirling, Phys. Lett. B252 (1990) 657;
S. Bethke et al., Nucl. Phys. B370 (1992) 310.

[11] T. Sjöstrand, Comp. Phys. Comm. 82 (1994) 74.

[12] S.Jadach, B.F.L. Ward, Z.Was, Comp. Phys. Comm. 79 (1994) 503;
CERN-TH-99-119, hep-ph/9905205 (1999).

[13] M. Skrzypek, S. Jadach, W. Placzek and Z. Was, Comp. Phys. Comm. 94 (1996) 216.

[14] G. Marchesini, B.R. Webber, G. Abbiendi, I.G. Knowles, M.H. Seymour, and L. Stanco, Comp. Phys. Comm. 67 (1992) 465.

[15] L. Lönnblad, Computer Physics Commun. 71 (1992) 15.

[16] S. Brandt et al., Phys. Lett. 12 (1964) 57;
E. Farhi, Phys. Rev. Lett. 39 (1977) 1587.

[17] T. Chandramohan and L. Clavelli, Nucl. Phys. B184 (1981) 365;
L. Clavelli and D. Wyler, Phys. Lett. B103 (1981) 383.

[18] P.E.L. Rakow and B.R. Webber, Nucl. Phys. B191 (1981) 63.

[19] G. Parisi, Phys. Lett. B74 (1978) 65;
J.F. Donoghue, F.E. Low, and S.Y. Pi, Phys. Rev. D20 (1979) 2759.

[20] R.K. Ellis, D.A. Ross and A.E. Terrano, Nucl. Phys. B178 (1981) 421.

[21] S. Catani et al., Phys. Lett. B263 (1991) 491;
Phys. Lett. B272 (1991) 368;
Nucl. Phys. B407 (1993) 3.

[22] G. Dissertori and M. Schmelling, Phys. Lett. B361 (1995) 167.

[23] S. Catani et al., Phys. Lett. B295 (1992) 269;
Yu.L. Dokshitzer et al., JHEP 1 (1998) 11.

[24] S. Catani et al., Phys. Lett. B427 (1998) 377.

[25] A. Banfi et al., JHEP 201 (2002) 18. e-Print Archive: hep-ph/0112156

[26] P. Nason and C. Oleari, Nucl. Phys. B521 (1998) 237.

[27] M. Dasgupta and G. P. Salam, DESY-01-160, LPTHE-01-43, hep-ph/0110213

[28] D. E. Groom et al, Eur. Phys. J. C15 (2000) 1.

[29] R. Barate et al., ALEPH Collab., Phys. Rep. 294 (1998) 1.

[30] D. Buskulic et al., ALEPH Collab., Z. Phys. C73 (1997) 409.

[31] R. Barate et al., ALEPH Collab., Z. Phys. C76 (1997) 1.

A Theoretical predictions

To second order in α_s, the distribution of a generic event-shape variable y is given by:

$$\frac{1}{\sigma_{tot}}\frac{d\sigma(y)}{dy} = \overline{\alpha}_s(\mu^2)A(y) + \left(\overline{\alpha}_s(\mu^2)\right)^2\left[A(y)2\pi b_0 \ln\left(\frac{\mu^2}{s}\right) + B(y)\right] \ , \tag{1}$$

$$\text{where } \overline{\alpha}_s = \frac{\alpha_s}{2\pi} \ , \ b_0 = \frac{33-2n_f}{12\pi} \ , \ \mu = \text{renormalisation scale.} \tag{2}$$

The coefficient functions A and B are obtained from integration of the ERT matrix elements. Consider the cumulative cross section (Radiator) :

$$R(y,\alpha_s) \equiv \frac{1}{\sigma_{tot}}\int_0^y \frac{d\sigma(x,\alpha_s)}{dx}dx \ , \tag{3}$$

which may be cast into the second-order form

$$R^{\mathcal{O}(\alpha_s^2)}(y,\alpha_s) = 1 + \mathcal{A}(y)\overline{\alpha}_s + \mathcal{B}(y){\overline{\alpha}_s}^2 \ , \tag{4}$$

where $\mathcal{A}$ and $\mathcal{B}$ are integrated forms of A and B, and the explicit scale dependence has been dropped for clarity.
The prediction of the **Log(R)** matching scheme is given by:

$$\begin{aligned} \ln R(y,\alpha_s) &= Lg_1(\alpha_s L) + g_2(\alpha_s L) - (G_{11}L + G_{12}L^2)\overline{\alpha}_s \\ &- (G_{22}L^2 + G_{23}L^3){\overline{\alpha}_s}^2 + \mathcal{A}(y)\overline{\alpha}_s + \left[\mathcal{B}(y) - \frac{1}{2}\mathcal{A}^2(y)\right]{\overline{\alpha}_s}^2 \ , \end{aligned} \tag{5}$$

with $L = \ln(1/y)$ for $y = 1-T, M_H^2/s, y_3, B_T, B_W$ and $L = \ln(6/C)$ for C-parameter. Expressions for the functions g_1 and g_2, which resum leading and next-to-leading logarithms to all orders in

α_s, can be found in the literature [21] [22] [23] [24] [25].
A kinematic constraint is imposed to the **modified Log(R)** matching scheme to guarantee that the prediction of the distribution vanishes at a given value y_{max}.

$$\ln R(y_{max}) = 0 \ , \ \left. \frac{1}{\sigma_{tot}} \frac{d\sigma(y)}{dy} \right|_{y=y_{max}} = \left. \frac{dR}{dy} \right|_{y=y_{max}} = 0 \ . \tag{6}$$

To fulfill this constraint L is replaced by $\tilde{L} = \frac{1}{p} \ln \left(\left(\frac{1}{y} \right)^p + (\frac{1}{y_{max}})^p + 1 \right)$, respectively $\tilde{L} = \frac{1}{p} \ln \left(\left(\frac{6}{C} \right)^p + (\frac{6}{C_{max}})^p + 1 \right)$ for C-parameter. The power p is usually chosen equal to unity, the case $p = 2$ is called second degree modification. The values of y_{max} and C_{max} are given in Table 7. Hence the prediction of the **modified Log(R)** matching scheme is simply obtained by

variable	$1-T$	M_H^2/s	$-\ln y_3$	B_T	B_W	C
y_{max}	0.5	0.47	$\ln 3$	0.41	0.35	1

Table 7: Values of y_{max} at which distributions are forced to vanish.

replacing L by $\tilde{L}$ in equation (5).
The expression for the **R** matching scheme reads as

$$\begin{aligned} R(y,\alpha_s) &= (1 + c_1\overline{\alpha}_s + c_2{\overline{\alpha}_s}^2) \exp\left[Lg_1(\alpha_s L) + g_2(\alpha_s L) + G_{21} L {\overline{\alpha}_s}^2 \right] \\ &- G_{21} L {\overline{\alpha}_s}^2 - \left[C_1 + G_{11} L + G_{12} L^2 \right] \overline{\alpha}_s \\ &- \left[C_2 + C_1(G_{11} L + G_{12} L^2) + \frac{1}{2}(G_{11} L + G_{12} L^2)^2 + (G_{22} L^2 + G_{23} L^3) \right] {\overline{\alpha}_s}^2 \\ &+ \mathcal{A}(y)\overline{\alpha}_s + \mathcal{B}(y){\overline{\alpha}_s}^2 \ . \end{aligned} \tag{7}$$

The constraints for the **modified R** matching are

$$R(y_{max}) = 1 \ , \ \left. \frac{1}{\sigma_{tot}} \frac{d\sigma(y)}{dy} \right|_{y=y_{max}} = \left. \frac{dR}{dy} \right|_{y=y_{max}} = 0 \ . \tag{8}$$

Here a simple modification of L does not satisfy the second constraint. Therefore, L is modified and the matching coefficients G_{11} and G_{21} become functions of y according to the condition:

$$\tilde{L}(y_{max}) = 0 \ , \ \tilde{G}_{11}(y_{max}) = 0 \ , \ \tilde{G}_{21}(y_{max}) = 0 \ . \tag{9}$$

This is achieved with the following modification:

$$\begin{aligned} \tilde{L}(y) &= \frac{1}{p} \ln \left[\left(\frac{1}{y} \right)^p + (\frac{1}{y_{max}})^p + 1 \right] \\ \tilde{G}_{11}(y) &= G_{11} \left[1 - \left(\frac{y}{y_{max}} \right)^p \right] \\ \tilde{G}_{21}(y) &= G_{21} \left[1 - \left(\frac{y}{y_{max}} \right)^p \right] \ , \end{aligned} \tag{10}$$

with the special case of C-parameter $\tilde{L}(C) = \frac{1}{p} \ln \left[(\frac{6}{C})^p + (\frac{6}{C_{max}})^p + 1 \right]$.
Finally the expression for the **modified R** matching scheme can be written as

$$\begin{aligned} \tilde{R}(y,\alpha_s) &= (1 + c_1\overline{\alpha}_s + c_2{\overline{\alpha}_s}^2) \exp\left[\tilde{L} g_1(\alpha_s \tilde{L}) + g_2(\alpha_s \tilde{L}) - \frac{y}{y_{max}} G_{11} \overline{\alpha}_s \tilde{L} + \tilde{G}_{21} \tilde{L} {\overline{\alpha}_s}^2 \right] \\ &- \tilde{G}_{21} \tilde{L} {\overline{\alpha}_s}^2 - \left[C_1 + \tilde{G}_{11} \tilde{L} + G_{12} \tilde{L}^2 \right] \overline{\alpha}_s \\ &- \left[C_2 + C_1(\tilde{G}_{11} \tilde{L} + G_{12} \tilde{L}^2) + \frac{1}{2}(\tilde{G}_{11} \tilde{L} + G_{12} \tilde{L}^2)^2 + (G_{22} \tilde{L}^2 + G_{23} \tilde{L}^3) \right] {\overline{\alpha}_s}^2 \\ &+ \mathcal{A}(y)\overline{\alpha}_s + \mathcal{B}(y){\overline{\alpha}_s}^2 \ . \end{aligned} \tag{11}$$

The resummation in terms of the logarithmic variable $L = \log \frac{1}{y}$ can be re-written in terms of a rescaled variable $\hat{L} = \log \frac{1}{y \cdot x_L}$. Such a rescaling alters the resummed formulae in the unmodified case according to :

$$\begin{aligned} L &= \log\left(\frac{1}{y}\right) \to \hat{L} = \log \frac{1}{y \cdot x_L} \\ g_1(\alpha_s L) &\to g_1(\alpha_s \hat{L}) \\ g_2(\alpha_s L) &\to g_2(\alpha_s \hat{L}) + \ln X \frac{d}{d\bar{L}} \left(\bar{L} g_1(\alpha_s \bar{L})\right) \ . \end{aligned} \tag{12}$$

For modified matching schemes the logarithmic variable L is replaced by :

$$\tilde{L} = \frac{1}{p} \ln \left[\left(\frac{1}{y}\right)^p - \left(\frac{1}{y_{max}}\right)^p + 1 \right] \to \hat{L} = \frac{1}{p} \ln \left[\left(\frac{1}{x_L \cdot y}\right)^p - \left(\frac{1}{x_L \cdot y_{max}}\right)^p + 1 \right] \tag{13}$$

Rescaling the logarithmic variable also entails changes to the fixed-order coefficients both in the modified and unmodified cases:

$$\begin{aligned} G_{12} &\to \hat{G}_{12} = G_{12} \\ G_{11} &\to \hat{G}_{11} = G_{11} + 2G_{12} \ln X \\ G_{23} &\to \hat{G}_{23} = G_{23} \\ G_{22} &\to \hat{G}_{22} = G_{22} + 3G_{23} \ln X \\ G_{21} &\to \hat{G}_{21} = G_{21} + 2G_{22} \ln X + 3G_{23} \ln^2 X \\ C_1 &\to \hat{C}_1 = C_1 + G_{11} \ln X + G_{12} \ln^2 X \\ C_2 &\to \hat{C}_2 = C_2 + (C_1 G_{11} + G_{21}) \ln X + (C_1 G_{12} + G_{22} + \tfrac{1}{2} G_{11}^2) \ln^2 X \\ &\qquad + (G_{23} + G_{12} G_{11}) \ln^3 X + \tfrac{1}{2} G_{12}^2 \ln^4 X \end{aligned} \tag{14}$$

In the case of the modified R matching scheme, the modified coefficients should be determined in terms of the unmodified ones. Factors of the type $\left[1 - \left(\frac{y}{y_{max}}\right)^p\right]$ and changes related to the renormalization scale are to be applied to the modified quantities.